# One-Step Low-Temperature Route for the Preparation of Electrochemically Active $LiMnPO_4$ Powders

C. Delacourt, P. Poizot, M. Morcrette, J.-M. Tarascon, and C. Masquelier*

*Laboratoire de Réactivité et de Chimie des Solides, CNRS UMR 6007, Université de Picardie Jules Verne, 33 Rue St. Leu, 80039 Amiens Cedex 9, France*

*Received July 30, 2003. Revised Manuscript Received October 23, 2003*

Pure and well-crystallized $LiMnPO_4$ powders were obtained by a direct precipitation route in an aqueous medium at 373 K. A thermodynamic study of the system $Li^+$/Mn(II)/phosphate/$H_2O$ identified a pH range in which $LiMnPO_4$ precipitation was the most probable. From these theoretical considerations, the olivine-type compound precipitation turned out to be straightforward, i.e., no further thermal treatment was needed. A systematic study of the influence of synthesis parameters enabled tailoring of the size of the as-obtained particles. The smallest precipitated particles (∼100 nm) led to a global improvement of the electrochemical behavior when used in lithium batteries, consisting in lowering the polarization and enhancement of the reversible capacities (∼70 mAh/g at C/20). A two-phase Li extraction/insertion mechanism was identified, using the potential intermittent titration technique (PITT) and in situ X-ray diffraction, between $LiMnPO_4$ and the delithiated phase $MnPO_4$, indexed in the space group *Pmnb* with unit cell parameters $a = 5.93(2)$ Å, $b = 9.69(6)$ Å, and $c = 4.78(1)$ Å.

## 1. Introduction

Among the known Li insertion compounds, the layered rock salt oxides $LiCoO_2$[1] and $LiNiO_2$,[2] and the spinel $LiMn_2O_4$[3,4] are now commercially used as 4-V positive electrode materials in rechargeable lithium batteries. However, such materials (namely the layered structures) suffer from poor chemical/electrochemical stability in their highly oxidized state,[5] and $LiMn_2O_4$ suffers from dissolution in the electrolyte leading to a rapid capacity fading under high-temperature storage.[6] Phosphate-based electrode materials, especially the phospho-olivines $LiMPO_4$ (where M = Fe, Mn, Co, Ni), are now recognized as attractive alternatives.[7] Beyond their high theoretical capacities (∼170 mAh·g$^{-1}$), the strong P−O covalent bonds drive the potential of the $M^{3+}/M^{2+}$ redox couple to values greater than 3.5 V vs $Li^+$/Li. Several groups succeeded in tailoring $LiFePO_4$/C composite electrodes approaching theoretical capacities at high rates of charge and discharge.[8−12] Therefore, because the gravimetric density (∼3.5 g.cm$^{-3}$) of $LiFePO_4$ is lower than that of $LiCoO_2$, its performance is still lower than that of the latter. To counterbalance such an effect the $LiMnPO_4$ phase is quite attractive owing to the potential of the $Mn^{3+}/Mn^{2+}$ redox couple located at 4.1 V vs $Li^+$/Li, and which is compatible with the electrolytes presently used in Li-ion batteries.

Besides the original work of Padhi,[7] only limited literature is available on $LiMnPO_4$ so far.[13,14] Padhi et al. noticed that extraction of lithium from $Li[Mn_yFe_{1-y}]PO_4$ compositions occurred at 3.4 V vs $Li^+$/Li and 4.1 V vs $Li^+$/Li for the $Fe^{3+}/Fe^{2+}$ and $Mn^{3+}/Mn^{2+}$ couples, respectively. The relative capacities associated with each of these redox couples are directly linked to the Fe and Mn contents in $Li[Mn_yFe_{1-y}]PO_4$. Therefore, for $y > 0.75$, the experimental capacity was found to be far below the expected one. More recently, Yamada et al. corroborated these results and tried to explain the large increase in the polarization overshoot to oxidize $Mn^{2+}$ for $y > 0.75$ as nested in the elastic tolerance limit of the delithiated form $[Mn_yFe_{1-y}]PO_4$ ($y > 0.75$). Indeed, strong electron ($Mn^{3+}$: $3d^4$) lattice interactions (Jahn−Teller effect) induce large anisotropic distortion in the $Fe^{3+}PO_4$−$Mn^{3+}PO_4$ binary system, and thus may limit the resulting solubility to $y < 0.8$.[13] Controversial results were communicated by another group from the same

* To whom correspondence should be addressed via e-mail at christian.masquelier@u-picardie.fr.

(1) Mizushima, K.; Jones, P. C.; Wiseman, P. C.; Goodenough, J. B. *Mater. Res. Bull.* **1980**, *15*, 783.
(2) Thomas, M. G. S. R.; David, W. I. F.; Goodenough, J. B.; Groves, P. *Mater. Res. Bull.* **1985**, *20*, 1137.
(3) Thackeray, M. M.; David, W. I. F.; Bruce, P. G.; Goodenough, J. B. *Mater. Res. Bull.* **1983**, *18*, 461.
(4) Thackeray, M. M.; Johnson, P. J.; de Picciotto, L. A.; Bruce, P. G.; Goodenough, J. B. *Mater. Res. Bull.* **1984**, *19*, 179.
(5) Dahn, J. R.; Fuller, E. W.; Obrovac, M.; Von Sacken, U. *Solid State Ionics* **1994**, *69*, 26.
(6) Blyr, A.; Sigala, C.; Amatucci, G.; Guyomard, D.; Chabre, Y.; Tarascon, J. M. *J. Electrochem. Soc.* **1998**, *145*, 194.
(7) Padhi, A. K.; Nanjundaswamy, K. S.; Goodenough, J. B. *J. Electrochem. Soc.* **1997**, *144* (4), 1188.
(8) Morcrette, M.; Wurm, C.; Gaubicher, J.; Masquelier, C. *Electrode Materials Meeting*, Bordeaux Arcachon, 27 May−1 June 2001.
(9) Ravet, N.; Goodenough, J. B.; Besner, S.; Simoneau, M.; Hovington, P.; Armand, M. *Joint International Meeting*, Hawaii, 17 Oct.−22 Oct. 1999.
(10) Yamada, A.; Chung, S. C.; Hinokuma, K. *J. Electrochem. Soc.* **2001**, *148* (3), A224−A229.
(11) Huang, H.; Yin, S.-C.; Nazar, L. F. *Electrochem. Solid State Lett.* **2001**, *4* (10), A170−A172.
(12) Franger, S.; Le Cras, F.; Bourbon, C.; Rouault, H. *Electrochem. Solid State Lett.* **2002**, *5* (10), A231−A233.
(13) Yamada, A.; Chung, S.-C. *J. Electrochem. Soc.* **2001**, *148* (8), A960.
(14) Li, G.; Azuma, H.; Tohda, M. *Electrochem. Solid State Lett.* **2002**, *5* (6), 135.

10.1021/cm030347b CCC: $27.50 
Published on Web 12/12/2003

corporation (Sony) on the electrochemical behavior of pure $LiMnPO_4$ powders: Li et al. reported on a stable reversible capacity greater than 140 $mAh{\cdot}g^{-1}$ at 0.28 $mA{\cdot}cm^{-2}$ for the two-phase reaction $LiMnPO_4$−$MnPO_4$.[14]

At this stage, one may reasonably argue that Yamada's and Li's results are in strong contradiction. Li's data suggest the thermodynamic existence of olivine-type $MnPO_4$, as shown by the well-defined two-phase plateau at 4.1 V vs $Li^+/Li$. Yamada's data, on the contrary, indicate the presence of a non-olivine phase for $y > 0.8$ in $[Mn_yFe_{1-y}]PO_4$. If $MnPO_4$ exists, the great overpotential observed by Padhi and Yamada for $y > 0.75$ is thus only due to ohmic polarization and/or kinetic effects such as charge transfer, front phase migration, etc. Bearing in mind Goodenough's statement[15] that care had to be taken in tailoring the preparation of small size particles of phospho-olivines for optimal performances, we decided to embark on a "chimie douce" route for the synthesis of $LiMnPO_4$ powders that had never been reported so far to our knowledge. The chosen method consisted of precipitation of $LiMnPO_4$ in an aqueous medium at low temperature. This enabled control of morphologies and sizes of the precipitated particles, by adjusting the thermodynamic (precursors concentrations, pH, temperature, etc.) and kinetic (reaction time, stirring rate, etc.) parameters.

In this paper, we report for the first time on the direct precipitation of fine $LiMnPO_4$ powders in an aqueous medium. Thermodynamic calculations were carried out in a first stage so as to predict the conditions at which pure $LiMnPO_4$ may be obtained. Powders with various morphologies and crystallinities were subsequently prepared and characterized by X-ray diffraction, BET, SEM, and TGA experiments. Chemical and electrochemical extraction/insertion of lithium from $LiMnPO_4$ was investigated through galvanostatic measurements, galvanostatic and potentiostatic intermittent titration techniques (GITT and PITT), and in situ X-ray diffraction.

## 2. Experimental Section

All the $LiMnPO_4$ powders were synthesized by precipitation in aqueous solutions made from deionized water. The precursors used were $Mn(NO_3)_2{\cdot}4H_2O$ (Merck, 98.5%), $H_3PO_4$ (Baker, 85%), $LiNO_3$ (Alfa Aesar, 99%), and $LiOH{\cdot}H_2O$ (Sigma Aldrich, 99%) to adjust the initial pH. The pH measurements were carried out using a pHM210 (Tacussel) pHmeter previously calibrated with standard solutions (pH = 4.00 ± 0.01 and pH = 7.00 ± 0.01, Sigma Aldrich). The precipitates were separated from the solutions by centrifugation or filtration, rinsed several times with deionized water, finally rinsed with acetone, and then dried at 55 °C for at least 1 day.

Chemical oxidation of $LiMnPO_4$ was performed using 3 equiv of nitronium tetrafluoroborate ($NO_2BF_4$, Aldrich) in acetonitrile in an environmentally controlled drybox at room temperature and under stirring.[16] Chemical lithiation of $Li_xMnPO_4$ was performed using 3 equiv of lithium iodide (LiI, Aldrich) in acetonitrile under air at room temperature and under stirring.

Morphology of the powders was observed by scanning electron microscopy (SEM) by means of a Philips FEG XL-30. A Micromeritics Gemini II 2370 analyzer with nitrogen as adsorption gas was used to perform the Brunauer−Emmett−Teller multipoint method[17] to determine the surface area ($S_{BET}$).

Thermal analyses were carried out under air using a Mettler TG50 apparatus with the TC11 interface. The atomic ratios Mn/P were checked by energy dispersive spectroscopy (EDS) with a Link Isis apparatus (Oxford). The atomic Li/Mn ratios were determined by atomic absorption spectroscopy using a Perkin-Elmer AAnalyst 300 piloted by AAWinlab software.

X-ray diffraction experiments (XRD) were performed using either a Philips PW 1710 diffractometer (Cu $K\alpha_{1,2}$ radiation, back monochromator) or a Bruker D8 diffractometer (Co $K\alpha_{1,2}$ radiation, equipped with a PSD or a scintillator detector). The D8 Bruker diffractometer was also used for in situ X-ray diffraction during charge/discharge of the positive electrode material. To this end, a modified swagelok cell equipped with a Be window was used as described in ref 18.

Electrochemical characterizations were carried out through galvanostatic and potentiostatic techniques in terms of charge−discharge potential profiles, using a VMP or a Macpile automatic cycling/data recording system (Biologic, S. A., Claix, France). Swagelok-type cells were assembled in an environmentally controlled drybox. The negative electrode was a disk of lithium metal foil. A Whattman GF/D borosilicate glass fiber sheet, soaked in a solution of 1 M $LiPF_6$ in EC/DMC (1:1 in weight), was placed between the 2 electrodes. The composite positive electrodes contained 16.7 wt % of acetylene black and 83.3 wt % of active material without binder and were directly deposited onto the aluminum collector. Intimate mixing between the active material and acetylene black had been ensured by ball-milling using a SPEX 8000 vertical ball-miller. The typical loading of positive electrode was around 14 mg per cell.

## 3. Thermodynamic Approach to $LiMnPO_4$ Precipitation

To find optimal conditions for $LiMnPO_{4\downarrow}$ precipitation in an aqueous medium, a detailed investigation of the thermodynamic properties of the system $Li^+/Mn(II)/$phosphate/$H_2O$ was done. To this end, the first step was inventorying the various species, which exist in the system, and that are reported in the literature: $H_3O^+$ (noted $H^+$), $OH^-$, $PO_4^{3-}$, $HPO_4^{2-}$, $H_2PO_4^-$, $H_3PO_4$, $Mn^{2+}$, $Mn(OH)^+$, $Mn(OH)_2$, $Mn(OH)_3^-$, $Mn(OH)_4^{2-}$, $Mn_2(OH)^{3+}$, $Mn_2(OH)_3^+$, and $MnHPO_4$ as soluble species, and $Mn(OH)_{2\downarrow}$, $MnHPO_{4\downarrow}$, $Mn_3(PO_4)_{2\downarrow}$, and $Li_3PO_{4\downarrow}$ as insoluble compounds.[19] This inventory leads to the 15 equilibria listed in Table 1, each of them giving rise to an equation from the mass action law, in which equilibrium constant values were taken from ref 19. Note that the equilibrium 16 is related to $LiMnPO_{4\downarrow}$ for which no Gibbs free energy value or solubility product is available in the literature. Equations 17−20 in Table 1 refer to possible mass balance relationships. In a second stage, various combinations of these equations were considered, depending on the nature of the solid phases that may be in equilibrium with the solution. As the number of these solid phases cannot exceed 2 (the variance being necessarily positive or equal to zero), and as we neglected first the equilibrium related to $LiMnPO_4$, 11 systems had to be considered (Table 2). Solutions of these 11 systems were easily found using the Newton−Raphson

(15) Goodenough, J. B.; Padhi, A. K.; Nanjundaswamy, K. S.; Masquelier, C. U.S. Patent 08/840,523, 1997.

(16) Wizansky, A. R.; Rauch, P. E.; Disalvo, F. J. *J. Solid State Chem.* **1989**, *81*, 203.

(17) Brunauer, S.; Emmett, P. H.; Teller, E. J. *J. Am. Chem. Soc.* **1938**, *60*, 309.

(18) Morcrette, M.; Chabre, Y.; Vaughan, G.; Amatucci, G.; Leriche, J.-B.; Patoux, S.; Masquelier, C.; Tarascon, J.-M. *Electrochim. Acta* **2002**, *47*, 3137−3149.

(19) Kotrlý, Šůcha, L. *Handbook of Chemical Equilibria in Analytical Chemistry*; Ellis Horwood Limited/John Wiley & Sons: New York, 1985.

**Table 1. Mass Action Law and Mass Balance Equations[a]**

Mass Action Law Equations

| eq no. | equilibrium reactions | symbol for constant | equation |
|---|---|---|---|
| 1 | $H_2O \leftrightarrows H^+ + OH^-$ | $K_w$ | $K_w = [H^+]\cdot[OH^-]$ |
| 2 | $HPO_4^{2-} \leftrightarrows PO_4^{3-} + H^+$ | $K_{h1}$ | $K_{h1} = [PO_4^{3-}]\cdot[H^+]/[HPO_4^{2-}]$ |
| 3 | $H_2PO_4^- \leftrightarrows HPO_4^{2-} + H^+$ | $K_{h2}$ | $K_{h2} = [HPO_4^{2-}]\cdot[H^+]/[H_2PO_4^-]$ |
| 4 | $H_3PO_4 \leftrightarrows H_2PO_4^- + H^+$ | $K_{h3}$ | $K_{h3} = [H_2PO_4^-]\cdot[H^+]/[H_3PO_4]$ |
| 5 | $Mn^{2+} + OH^- \leftrightarrows Mn(OH)^+$ | $\beta_1$ | $\beta_1 = [Mn(OH)^+]/\{[Mn^{2+}]\cdot[OH^-]\}$ |
| 6 | $Mn^{2+} + 2\ OH^- \leftrightarrows Mn(OH)_2$ | $\beta_2$ | $\beta_2 = [Mn(OH)_2]/\{[Mn^{2+}]\cdot[OH^-]^2\}$ |
| 7 | $Mn^{2+} + 3\ OH^- \leftrightarrows Mn(OH)_3^-$ | $\beta_3$ | $\beta_3 = [Mn(OH)_3^-]/\{[Mn^{2+}]\cdot[OH^-]^3\}$ |
| 8 | $Mn^{2+} + 4\ OH^- \leftrightarrows Mn(OH)_4^{2-}$ | $\beta_4$ | $\beta_4 = [Mn(OH)_4^{2-}]/\{[Mn^{2+}]\cdot[OH^-]^4\}$ |
| 9 | $2\ Mn^{2+} + OH^- \leftrightarrows Mn_2(OH)^{3+}$ | $\beta_{12}$ | $\beta_{12} = [Mn_2(OH)^{3+}]/\{[Mn^{2+}]^2\cdot[OH^-]\}$ |
| 10 | $2\ Mn^{2+} + 3\ OH^- \leftrightarrows Mn_2(OH)_3^+$ | $\beta_{32}$ | $\beta_{32} = [Mn_2(OH)_3^+]/\{[Mn^{2+}]^2\cdot[OH^-]^3\}$ |
| 11 | $Mn^{2+} + HPO_4^{2-} \leftrightarrows MnHPO_4$ | $K(MnHPO_4)$ | $K(MnHPO_4) = [MnHPO_4]/\{[Mn^{2+}]\cdot[HPO_4^{2-}]\}$ |
| 12 | $Mn(OH)_2\downarrow \leftrightarrows Mn^{2+} + 2\ OH^-$ | $K_s(Mn(OH)_2)$ | $K_s(Mn(OH)_2) = [Mn^{2+}]\cdot[OH^-]^2$ |
| 13 | $MnHPO_4\downarrow \leftrightarrows Mn^{2+} + HPO_4^{2-}$ | $K_s(MnHPO_4)$ | $K_s(MnHPO_4) = [Mn^{2+}]\cdot[HPO_4^{2-}]$ |
| 14 | $Mn_3(PO_4)_2\downarrow \leftrightarrows 3\ Mn^{2+} + 2\ PO_4^{3-}$ | $K_s(Mn_3(PO_4)_2)$ | $K_s(Mn_3(PO_4)_2) = [Mn^{2+}]^3\cdot[PO_4^{3-}]^2$ |
| 15 | $Li_3PO_4\downarrow \leftrightarrows 3\ Li^+ + PO_4^{3-}$ | $K_s(Li_3PO_4)$ | $K_s(Li_3PO_4) = [Li^+]^3\cdot[PO_4^{3-}]$ |
| 16 | $LiMnPO_4\downarrow \leftrightarrows Li^+ + Mn^{2+} + PO_4^{3-}$ | $K_s(LiMnPO_4)$ | $K_s(LiMnPO_4) = [Li^+]\cdot[Mn^{2+}]\cdot[PO_4^{3-}]$ |

Mass Balance Equations

| eq no. | equation |
|---|---|
| 17 | $[Mn(II)]^i_{tot} = [Mn^{2+}] + [Mn(OH)^+] + [Mn(OH)_2] + [Mn(OH)_3^-] + [Mn(OH)_4^{2-}] + 2\ [Mn_2(OH)^{3+}] + 2\ [Mn_2(OH)_3^+] + [MnHPO_4]$ |
| 18 | $[Phosphate]^i_{tot} = [PO_4^{3-}] + [HPO_4^{2-}] + [H_2PO_4^-] + [H_3PO_4] + [MnHPO_4]$ |
| 19 | $[Mn(II)]^i_{tot} - [Mn(II)]_{tot} = [Phosphate]^i_{tot} - [Phosphate]_{tot}$ |
| 20 | $[Mn(II)]^i_{tot} - [Mn(II)]_{tot} = 3/2.\{[Phosphate]^i_{tot} - [Phosphate]_{tot}\}$ |

[a] $[Mn(II)]^i_{tot}$ and $[Phosphate]^i_{tot}$ designate the initial total concentrations of Mn(II) and phosphate before the precipitation of solid phases, respectively. $[Mn(II)]_{tot}$ and $[Phosphate]_{tot}$ designate the total concentrations of Mn(II) and phosphate in equilibrium conditions, respectively.

**Table 2. Systems of Equations Depending on the Nature of the Solid Phase(s)**

| system no. | solid phase(s) | eq. considered |
|---|---|---|
| I | No solid phases | (1−11) + 17 + 18 |
| II | $Mn(OH)_2\downarrow$ | (1−11) + 12 + 18 |
| III | $MnHPO_4\downarrow$ | (1−11) + 13 + 19 |
| IV | $Mn_3(PO_4)_2\downarrow$ | (1−11) + 14 + 20 |
| V | $Li_3PO_4\downarrow$ | (1−11) + 15 + 17 |
| VI | $Mn(OH)_2\downarrow + MnHPO_4\downarrow$ | (1−11) + 12 + 13 |
| VII | $Mn(OH)_2\downarrow + Mn_3(PO_4)_2\downarrow$ | (1−11) + 12 + 14 |
| VIII | $Mn(OH)_2\downarrow + Li_3PO_4\downarrow$ | (1−11) + 12 + 15 |
| IX | $MnHPO_4\downarrow + Mn_3(PO_4)_2\downarrow$ | (1−11) + 13 + 14 |
| X | $MnHPO_4\downarrow + Li_3PO_4\downarrow$ | (1−11) + 13 + 15 |
| XI | $Mn_3(PO_4)_2\downarrow + Li_3PO_4\downarrow$ | (1−11) + 14 + 15 |
| XII | $LiMnPO_4\downarrow$ | (1−11) + 16 + 19 |
| XIII | $LiMnPO_4\downarrow + Mn(OH)_2\downarrow$ | (1−11) + 16 + 12 |
| XIV | $LiMnPO_4\downarrow + MnHPO_4\downarrow$ | (1−11) + 16 + 13 |
| XV | $LiMnPO_4\downarrow + Mn_3(PO_4)_2\downarrow$ | (1−11) + 16 + 14 |
| XVI | $LiMnPO_4\downarrow + Li_3PO_4\downarrow$ | (1−11) + 16 + 15 |

algorithm for equations with a degree ≥ 3. For each system of equations, the room temperature aqueous system was also completely defined for each pH value.

Among all the calculated possibilities (i.e., the 11 systems of equations), the most thermodynamically stable one, at a given value of pH, corresponds to the lowest total Mn(II) and phosphate concentrations. Figures 1a and b show the distribution diagram of soluble and solid species and the solubility diagram for Mn(II) and phosphate, respectively. For 0 ≤ pH ≤ 10.2, $MnHPO_4\downarrow$ should be the stable single phase, with its solubility that decreases as the pH increases. For 10.2 ≤ pH ≤ 10.7, a two-phase domain of $MnHPO_4\downarrow + \epsilon\ Li_3PO_4\downarrow$ is defined. For pH ≥ 10.7, another two-phase domain, where $Mn(OH)_2\downarrow$ and $Li_3PO_4\downarrow$ coexist (1/1 in molar ratio), was found. Note that no stability domain of $LiMnPO_4\downarrow$ appears from Figure 1, as no thermodynamic data were available for it. To overcome this, we used a simple approach considering the solubility behaviors of individual metal phosphates, i.e., $MnHPO_4\downarrow$ and $Li_3PO_4\downarrow$. By extrapolation to what is generally observed for mixed oxides and hydroxides,[20] we considered that the mixed phosphate $LiMnPO_4\downarrow$ would be more thermodynamically stable than the phosphates formed by each cation. As a consequence, the most probable domain of pH for the precipitation of $LiMnPO_4\downarrow$ was identified as the one where $MnHPO_4\downarrow$ and $Li_3PO_4\downarrow$ are simultaneously present: 10.2 ≤ pH ≤ 10.7. Note that this approach previously led to successful results for the coprecipitation of pure $Pb(Zr_{0.52}Ti_{0.48})O_3$ (PZT)[21] and several hydrated iron vanadates.[22]

A second and less intuitive alternative approach was successfully used to predict the precipitation domain of $LiMnPO_4\downarrow$. It consisted in taking into account the thermodynamic existence of $LiMnPO_4\downarrow$ (eq 16 in Table 1) that generated 5 additional systems of equations (Systems XII to XVI in Table 2). We then attributed a series of hypothetical solubility products values to equilibrium 16 in order to determine the narrowest pH range leading to a precipitation domain for $LiMnPO_4\downarrow$. For p*K*s = 16, we obtained, according to the same general procedure described above, the solubility diagrams of Figure 2. This value corresponds to the smallest integer value of p*K*s below which no domain of stability for $LiMnPO_4\downarrow$ may be found. Note that choosing a higher p*K*s would have resulted in increasing the theoretical pH range of $LiMnPO_4\downarrow$ stability, which is, as mentioned earlier, of poor interest: 8.36 ≤ pH ≤ 11.86 for p*K*s = 17 and 7.54 ≤ pH ≤ 12.37 for p*K*s = 18. For $Ks = 10^{-16}$, as seen on Figure 2, two domains are clearly separated in the pH range 9.4−11.35. $LiMnPO_4\downarrow$ precipitates as a single-phase from pH = 9.4−10.6 and is accompanied with $\epsilon\ Li_3PO_4\downarrow$ from pH = 10.6−

(20) Jolivet, J.-P. *De la solution à l'oxyde*; Interédition: Paris, 1994.
(21) Choy, J. H.; Han, Y. S.; Kim, J. T. *J. Mater. Chem.* **1995**, *5*, 65.
(22) Poizot, P.; Laruelle, S.; Touboul, M.; Tarascon, J.-M.; *C. R. Chimie* **2003**, 125−134.

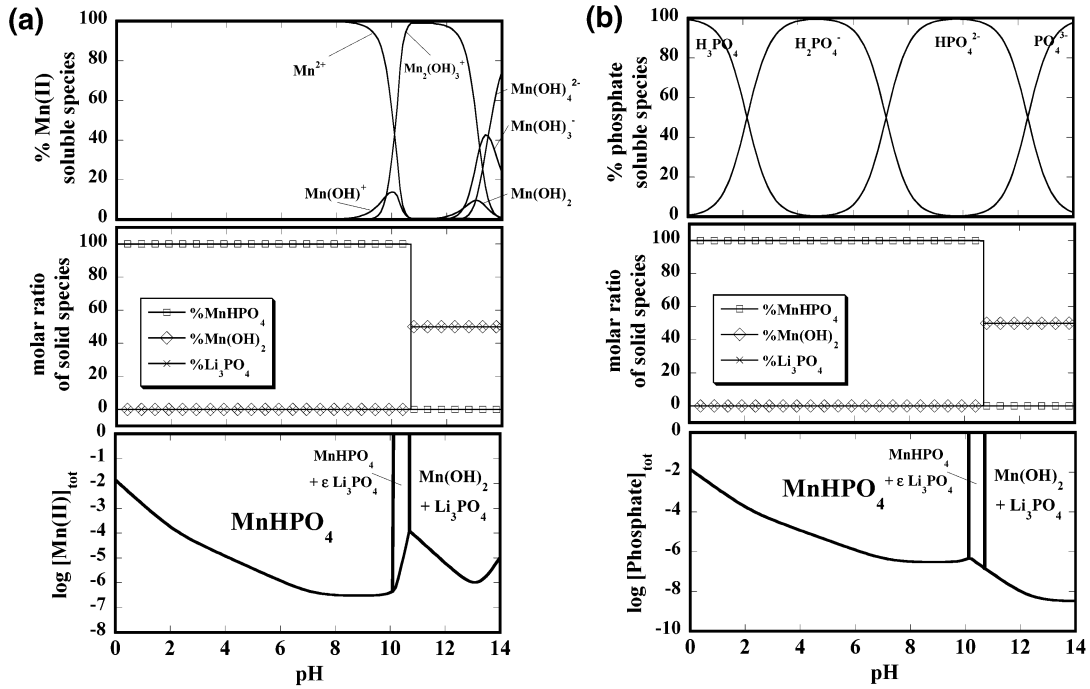


**Figure 1.** Top: Mn(II) (a) and phosphate (b) soluble species distribution diagrams. Center: solid species distribution diagram (molar ratio). Bottom: Mn(II) (a) and phosphate (b) solubility diagrams. Conditions: $[Mn(II)]^i_{tot} = [Phosphate]^i_{tot} = 0.1$ mol·L$^{-1}$; $[Li^+] = 1$ mol·L$^{-1}$.

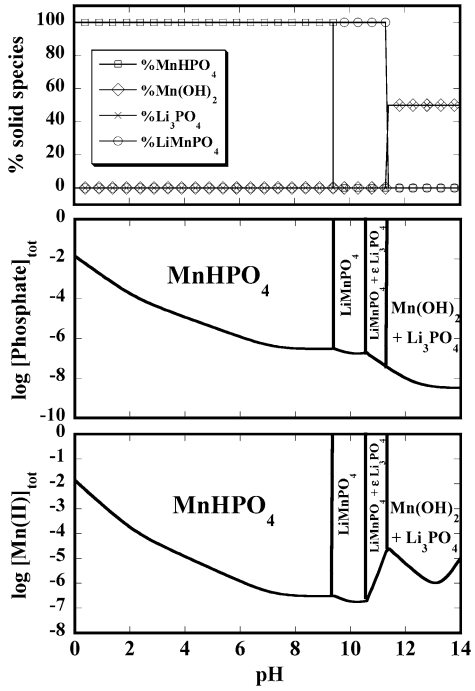


**Figure 2.** Top: solid species distribution diagram (molar ratio) with the hypothesis p$K$s($LiMnPO_4$) = 16. Phosphate (center) and Mn(II) (bottom) solubility diagrams with the hypothesis p$K$s($LiMnPO_4$) = 16. Conditions: $[Mn(II)]^i_{tot} = [Phosphate]^i_{tot} = 0.1$ mol·L$^{-1}$; $[Li^+] = 1$ mol·L$^{-1}$.

11.35. This approach is in very good agreement with the former one that led to a hypothetical pH range of 10.2−10.7.

As a remark, we ignored the ionic strength effects ($I_c$) by systematically choosing data given for $I_c = 0$ (at which a maximum of constants are available). For the same reason, calculations were performed considering standard conditions, $P = 10^5$ Pa and $T = 298.15$ K. Variations of thermodynamic constants of equilibria occur with temperature, but the main conclusions obtained at RT remain mostly valid up to ∼373 K. Thermodynamic calculations were done for initial concentrations of 0.1 mol·L$^{-1}$ for Mn(II) and phosphate. The concentration of the third species, $Li^+$, was chosen as 1 mol·L$^{-1}$ (large excess) in order to overpass diffusion limitations and to favor $LiMnPO_4\downarrow$ kinetics of precipitation of $LiMnPO_4\downarrow$. This strategy was successfully used for the precipitation of $LiNiVO_4\downarrow$.[23]

## 4. Synthesis Aspects

From the thermodynamic study reported above, and without considering the kinetics of the reactions taking place in the system, we determined that an alkaline pH around 10.5 was needed to precipitate $LiMnPO_4$. The formation of a solid phase is commonly described by 3 distinct steps comprising nucleation, growth, and aging. A strict control of the kinetics of each step enables, through the use of small concentrations of precursors, precipitation of crystalline phases, in particular by reducing the nucleation rate and favoring the aging step.

To conduct the synthesis, the pH of a limpid solution containing 0.02 mol·L$^{-1}$ Mn(II), 0.02 mol·L$^{-1}$ phosphate, and an excess of $Li^+$ ions (0.4 mol·L$^{-1}$) was raised slowly to the value of 10.7 at $T = 298$ K by addition of a 1 mol·L$^{-1}$ solution of LiOH. After 5 d of reaction under reflux conditions, to favor the aging step, a brownish precipitate was recovered that corresponds to a pure $LiMnPO_4$ powder (P/Mn ∼0.98 by EDS measurement) with relatively high crystallinity (Figure 3a). The X-ray diffraction pattern was fully indexed in the space group *Pmnb* with the cell parameters $a = 6.090(3)$ Å, $b =$

(23) Orsini, F.; Baudrin, E.; Denis, S.; Dupont, L.; Touboul, M.; Guyomard, D.; Piffard, Y.; Tarascon, J.-M. *Solid State Ionics* **1998**, *107*, 123−133.

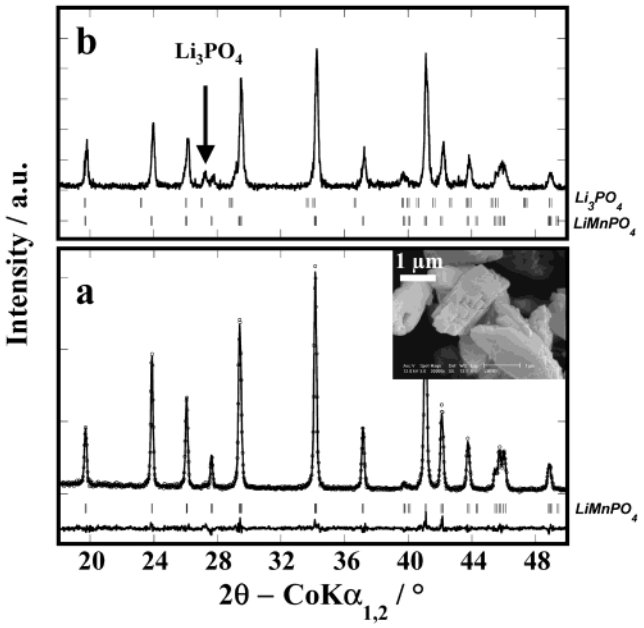


**Figure 3.** X-ray diffraction pattern for "thermodynamic conditions" pure $LiMnPO_4$ (a) (step 0.02°, acquisition time 12 s), and impure $LiMnPO_4$ obtained in higher concentrations conditions (b) (step 0.02°, acquisition time 1 s). Insert: SEM micrograph (×20 000) displaying the morphology and size of the pure $LiMnPO_4$ particles.

10.442(4) Å, and $c = 4.745(2)$ Å. Under these synthesis conditions, the BET surface of the $LiMnPO_4$ powder obtained by direct precipitation in aqueous medium was found to be smaller than 1 $m^2 \cdot g^{-1}$. SEM observations (inset of Figure 3a) revealed a particle size of 1−2 $\mu$m. TGA analysis under air indicated only a small weight loss of 3% at around 500 °C, which remains up to now unexplained.

As mentioned by Goodenough,[15] phosphate materials are poor electronic conductors, and small grain sizes are expected to improve the electrochemical properties. Having determined that pH ∼10.7 was the optimal thermodynamic condition for the precipitation of $LiMnPO_4$, our second approach to lower the particle size of the precipitate was to act on the kinetic parameters such as the concentrations of the different species. Increasing the precursors' concentrations generally enhances the nucleation rate and thus increases the number of nuclei. To this end, a 2 mol·$L^{-1}$ solution of LiOH was slowly added at 298 K to a limpid solution containing 0.1 mol·$L^{-1}$ Mn(II), 0.1 mol·$L^{-1}$ phosphate, and an excess of $Li^+$ ions (1 mol·$L^{-1}$) until pH = 10.1. After 5 d under reflux conditions, a brownish precipitate was recovered, which contained both $LiMnPO_4$ and $Li_3PO_4$ (Figure 3 b). This result was corroborated by atomic absorption measurements that revealed a Li/Mn atomic ratio of 1.2. Under these high-concentration conditions, thermodynamic calculations of Figure 2 indicate that $Li_3PO_4$ is metastable. Its experimental formation occurred because the medium (high concentrations, $T$ ∼298 K during LiOH addition...) favors the precipitation of "kinetic" phases that are very long to dissolve. Lowering the pH (initial pH fixed to 9.5 by reducing the amount of LiOH added) had no significant effect on the presence of $Li_3PO_4$. The problem was solved by adding LiOH to the initial mix of the precursors under reflux conditions ($T$ ∼373 K) and not at 298 K as developed above.

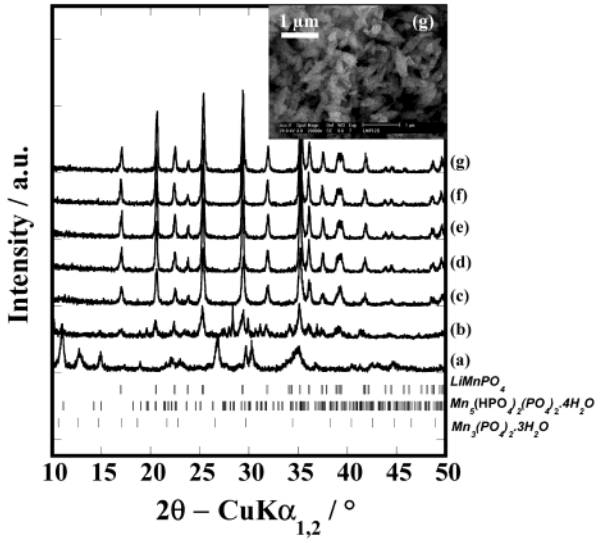


**Figure 4.** X-ray diffraction patterns of the precipitated phases at different reaction times in "rapid nucleation conditions" (step 0.02°, acquisition time 1 s) (a) 5 min, (b) 1 h, (c) 2 h, (d) 18 h, (e) 42 h, (f) 66 h, and (g) 90 h. Insert: SEM micrograph (×20 000) displaying the morphology and size of sample (g).

Under reflux conditions, the precipitation of $Li_3PO_4$ was successfully avoided. We report in Figure 4 the evolution of the X-ray diffraction patterns of the precipitates recovered at different reaction times, from 5 min to 90 h. None of the patterns exhibit the Bragg reflections of $Li_3PO_4$, even for the shorter times. The first compound to precipitate (within ∼5 min) is $Mn_3(PO_4)_2{\cdot}3H_2O$ (ICDD card No. 03-0426). $LiMnPO_4$ is formed after 1 h of reaction, together with another manganese phosphate, the hureaulite (ICDD card No. 86-1521) of formula $Mn_5(HPO_4)_2(PO_4)_2{\cdot}4H_2O$. After 2 h of reaction, $LiMnPO_4$ is the only insoluble phase formed. The half-height width B(2$\theta$) of the diffraction peaks diminishes as the reaction time increases, which can be directly linked to an enhancement of the crystallites' size. Simulations were made using the Winplotr-Fullprof suite[24] and a progressive increase in the isotropic crystallite size from ∼300 to ∼400 Å for sample c (∼2-h reaction) to sample g (∼4-d reaction) was found. Interestingly, we observed no significant changes of the particles' size, between 100 and 200 nm (insert of Figure 4), with the reaction time. BET measurements are in good agreement with the SEM observations and indicate a specific surface area of 23 $m^2 \cdot g^{-1}$ for the 2-h-aged sample and 13 $m^2 \cdot g^{-1}$ for the 4-d-aged sample. The latter method enables the synthesis of pure and small-particle-size $LiMnPO_4$. Our results indicate that the precipitation of $LiMnPO_4$ is not straightforward, as at least two unstable "kinetic" manganese phosphates are formed intermediary.

To conclude, this "chimie douce", robust, and low-cost method is perfectly adapted to obtain pure and well-crystallized $LiMnPO_4$. Varying the thermodynamic and kinetic parameters results in a large range of particle and crystallite sizes, as illustrated in Figure 5. These powders were then evaluated and compared as positive electrodes in lithium cells vs. Li extraction/insertion.

(24) Rodríguez-Carvajal, J. *J. Physica B* **1993**, *192*, 55.

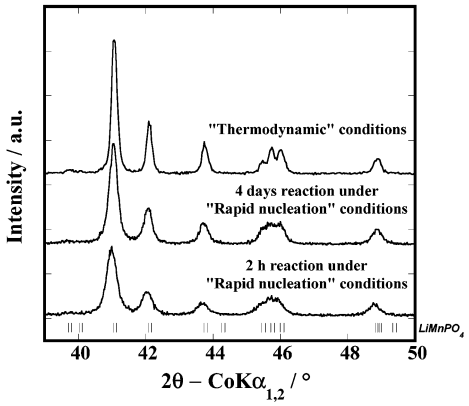


**Figure 5.** X-ray diffraction patterns of different crystallite-size $LiMnPO_4$ obtained in various precipitation conditions (step 0.02°, acquisition time 12 s).

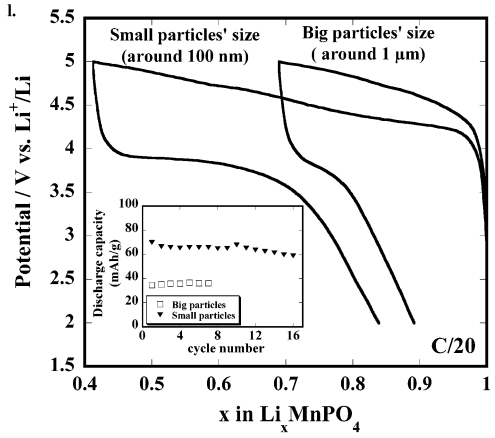


**Figure 6.** Potential−composition curves (C/20) of 2 different particle-size $LiMnPO_4$ (16.7 wt % carbon black, ball-milled 30 min). Insert: Capacity retention at C/20 for these 2 materials.

## 5. Electrochemical Properties

$LiMnPO_4$/carbon composite materials were tested vs lithium extraction/insertion in the potential range 2−4.5 or 2−5 V vs. $Li^+$/Li. To generate an efficient conductive carbon coating at the surface of the phosphate particles, the powders were ground with acetylene black in a way similar to what we previously described for $Li_3Fe_2(PO_4)_3$[25] and $LiFePO_4$.[8]

Figure 6 shows that small particles of $LiMnPO_4$ (obtained via the "rapid nucleation conditions") lead to a lower total polarization than bigger particles obtained under "thermodynamic conditions". This limits the electrolyte oxidation, which takes place for the upper values of potentials[26] and then leads to a large increase in the reversible specific capacity of the cell. All our further electrochemical characterizations were carried out with the small particle size (∼100 nm) sample.

Adjusting the duration of the ball-milling of $LiMnPO_4$/carbon composite electrodes is of great importance to provide an efficient conducting carbon coating at the surface of the active material. This procedure may be detrimental to the performances though as agglomerates generally form and highly divided powders may react with the electrolyte, or catalyze its oxidation at high potential. For the first discharge, the best performance we obtained was for a composite electrode ball-milled for 45 min (Figure 7). Interestingly, the discharge capacities of the electrodes ball-milled for more than 30 min increase slightly for the first 4 cycles. This phenomenon is more pronounced for the 90-min ball-milled sample, which is probably nested in an electrochemical grinding of $LiMnPO_4$/C agglomerates.

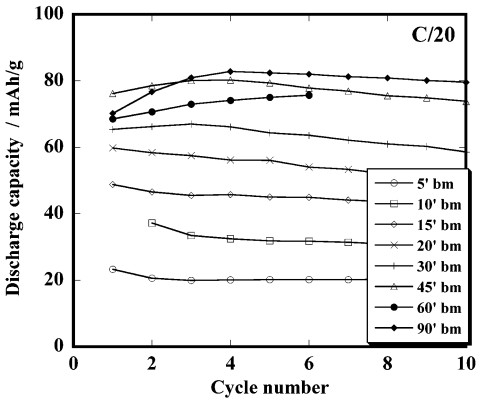


**Figure 7.** Capacity retention at C/20 for different ball-milling times with 16.7 wt % carbon black.

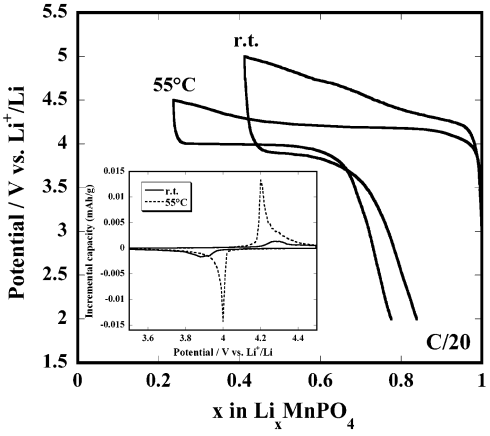


**Figure 8.** Potential−composition curves (C/20) of $LiMnPO_4$ (16.7 wt % carbon black, ball-milled 30 min) at RT and 55 °C. Insert: Incremental capacity of $LiMnPO_4$ (16.7 wt % carbon black, 30 min ball-milling) calculated from PITT measurements carried out at RT and 55 °C.

At this point, the best experimental capacity is still only limited to ∼70 $mAh{\cdot}g^{-1}$ at C/20 and ∼50 $mAh{\cdot}g^{-1}$ at C/5 (between 2 and 5 V vs $Li^+$/Li). Several components, such as electronic and ionic conductivity, as well as the charge-transfer rate and the front phase migration, may be at the origin of the high polarization of the cell. As seen on Figure 8, temperature has a major impact on these electric and/or kinetic contributions, and thus on the global behavior of the cell. Further work is in progress to fully discriminate the weight of each factor.

To further gain a better understanding of the Li extraction/insertion mechanism within this compound, potentiostatic intermittent titration technique (PITT) and in situ X-ray diffraction experiments were conducted. The PITT data reproduced on Figure 9 clearly illustrate (i) an electrochemical reaction that occurs mostly on discharge between 4.0 and 3.8 V vs $Li^+$/Li, and (ii) a current response typical of a two-phase process: the shape of the current decay vs time at each potential step is characteristic of the nucleation and

(25) Morcrette, M.; Wurm, C.; Masquelier, C. *Solid State Sci.* **2002**, *4*, 239−246.
(26) Blomgren, G. E. *J. Power Sources* **1999**, *81*−*82*, 112−118.

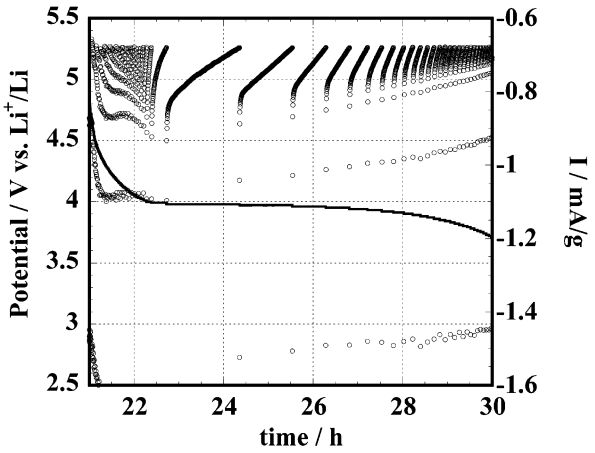


**Figure 9.** PITT measurements (with $|I_{lim}| = C/20$) for $LiMnPO_4$ at 55 °C (16.7 wt % carbon black, ball-milled 30 min).

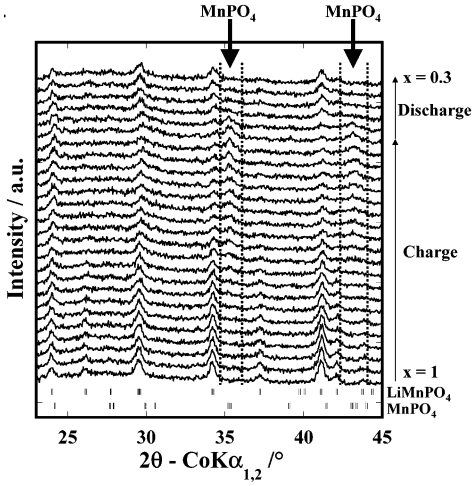


**Figure 10.** In situ X-ray diffraction measurements for $LiMnPO_4$ (16.7 wt % carbon black, 30 min ball-milling) (step 0.04°, acquisition time 4 s).

growth of a second phase. The potential of this first-order phase transition is equal to 4.10 V vs $Li^+/Li$, at both RT and 55 °C, as determined from the data plotted in the insert of Figure 8. An important issue, arising from Li's and Yamada's contradictory papers, was to try to get further insight into the real existence of the completely delithiated form $MnPO_4$. The X-ray diffraction data recorded in situ during the electrochemical extraction of Li from $LiMnPO_4$ are presented in Figure 10. The diffraction peaks of $LiMnPO_4$ progressively vanish while the intensities of several diffuse Bragg reflections increase on charge. At the end of charge though, the pristine $LiMnPO_4$ has not completely disappeared. We could index the XRD peaks of the growing phase in the space group *Pmnb* with unit cell parameters $a = 5.93(2)$ Å, $b = 9.69(6)$ Å, and $c = 4.78(1)$ Å, this leads to an anisotropic shrinkage of 8.9% (302(1) $Å^3$ for $LiMnPO_4$ to 275(1) $Å^3$ for $MnPO_4$). These values are in very good agreement with those reported for the mineral purpurite (ICDD card No. 77-0180) of formula $MnPO_4$. Interestingly, this also corresponds to the values one would obtain by extrapolating to $y = 1$ the evolution of the cell parameters of the $Mn_yFe_{1-y}PO_4$ solid solution given by Yamada et al.[13] In concordance with the existence of the mineral purpurite, our experiment tends to prove then the thermodynamic stability of $MnPO_4$. This is in contradiction with Yamada's report

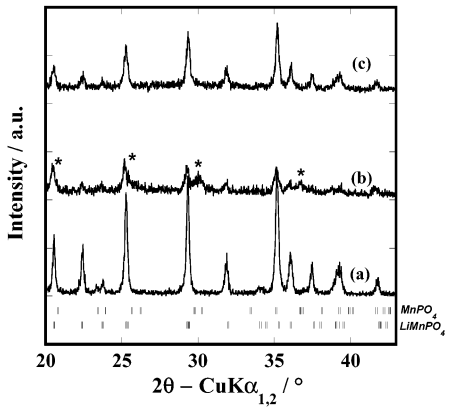


**Figure 11.** X-ray diffraction patterns of the (a) initial $LiMnPO_4$, (b) phase obtained after 1 d delithiation ($Li/Mn = 0.38$), (c) phase obtained after relithiation ($Li/Mn = 0.91$) (step 0.02°, acquisition time 1 s). Asterisks (*) indicate Bragg reflections of poorly-crystallized $MnPO_4$.

on the instability of $Mn_yFe_{1-y}PO_4$ for $y \geq 0.67$, due to the Jahn−Teller effect of $Mn^{3+}$ in the olivine-type structure.[27]

By chemical oxidation (8 d of reaction with $NO_2BF_4$ in acetonitrile), we obtained a purple powder of global composition $Li_{0.34}MnPO_4$ as determined by atomic absorption analysis. In the same way, relithiation of the partially delithiated powder led to the global composition $Li_{0.91}MnPO_4$. As shown by the XRD patterns of Figure 11, the oxidative reaction is not complete, as Bragg reflections of $LiMnPO_4$ are still present, even after 8 d of reaction. This limitation, which cannot be of thermodynamic origin with regard to the high potential of $NO_2^+/NO_2$ (5.1 V vs $Li^+/Li$ in acetonitrile), is probably due to kinetic limitations with regards to a low electronic and/or ionic conductivity of $MnPO_4$, which may constitute an insulating layer around the nremaining $LiMnPO_4$. Wide reflections of the olivine-type $MnPO_4$ suggest a much lower crystallinity for the delithiated phase, as previously observed for the electrochemical oxidation.

## 6. Conclusion

$LiMnPO_4$ was prepared by a direct precipitation method, in well-defined conditions first predicted by thermodynamic calculations. This "chimie douce" method, that has never been reported before to our knowledge, allowed the preparation of small particles that enhanced the electrochemical performances when used as positive electrodes in secondary lithium cells. Apart from Li's controversial communication,[14] it is the first time that such a reversible capacity (∼70 $mAh \cdot g^{-1}$ at C/20 and RT) is observed from pure $LiMnPO_4$. A two-phase process between the olivine-type $LiMnPO_4$ and the delithiated form $MnPO_4$ is proposed. Improving material properties to enhance electrochemical performances will be a necessary step to promote this compound as a positive material for lithium-ion batteries.

**Acknowledgment.** We thank Dr. D. Larcher for atomic absorption spectroscopy measurements and Dr. S. Patoux for fruitful scientific discussions.

CM030347B

(27) Yamada, A.; Kudo, Y.; Liu, K.-Y. *J. Electrochem. Soc.* **2001**, *148* (10), A1153−A1158.